Journal of Solid State Chemistry 183 (2010) 2161–2165

Contents lists available at ScienceDirect

Journal of Solid State Chemistry

journal homepage: www.elsevier.com/locate/jssc

Synthesis and luminescence properties of Yb^{3+} and Er^{3+} doped $KLa(WO_4)_2$ nanoparticles

Meng Chen [a], Tongqing Sun [b,*], Hong Chen [a], Yu Zhang [b], Li Wu [b], Yongfa Kong [a], Jingjun Xu [a,b]

[a] The MOE Key Laboratory of Weak-Light Nonlinear Photonics and TEDA Applied Physics School, Nankai University, Tianjin 300457, China
[b] School of Physics, Nankai University, Tianjin 300071, China

ARTICLE INFO

Article history:
Received 20 April 2010
Received in revised form
3 July 2010
Accepted 7 July 2010
Available online 15 July 2010

Keywords:
Pechini method
Upconversion luminescence
Nanocrystalline
Potassium lanthanum tungstate

ABSTRACT

The luminescent nanocrystalline Yb^{3+} and Er^{3+} codoped $KLa(WO_4)_2$ has been prepared by Pechini method. X-ray diffraction and transmission electron microscope were used to study the structure of the obtained samples. The average grain size of these samples depended on the annealing temperature, increasing with the increase of the temperature. The cell parameters and the crystallite size of $KYb_xEr_{0.02}La_{0.98-x}(WO_4)_2$ nanocrystalline decreased with the increase of x value. Luminescence studies showed that the intensity of upconversion emission of the Yb^{3+} and Er^{3+} codoped samples was much stronger than that of the Er^{3+} single doped samples (pumped by 980 nm LD). The upconversion emission mechanisms suggested that all the three bands of upconversion emissions were two-photon process.

1. Introduction

$KLa(WO_4)_2$ (KLW) is a member of double alkaline rare-earth tungstates with the general formula $ALn(WO_4)_2$, where A=Na or K and Ln is a lanthanide ion. These materials have widespread applications in the quantum electronics field [1–3]. Over the years, researchers have paid great attentions on the single crystal of these materials in order to take advantage of their laser properties. But in recent years, it has been revealed that the materials with grain size less than 100 nm exhibited different properties from conventional microcrystalline specimens [4–7]. Many kinds of luminescent materials have been prepared in nanocrystalline state by various methods [8–10].

KLW crystallizes in tetragonal $I4_1/a$ structure with two molecules per unit-cell, and the lattice parameters are $a=b=5.477$ Å, $c=12.080$ Å. In the KLW compound, La ions join by means of La–O–W–O–La, and K^+ ions and La^{3+} ions occupy alternately the same crystallographic position [11]. This structure results in a weaker interaction among the activators which occupy the La^{3+} sites and a lower fluorescence concentration quenching [12,13]. According to the energy level diagram, Er^{3+} ions can emit three bands of upconversion (UC) emissions in visible spectra and one band of downconversion (DC) emission at 1.54 μm excited by 980 nm LD, and all the four emissions are useful in laser domain. Yb^{3+} ions can be used as sensitizer for Er^{3+} ions. Furthermore, all the La^{3+}, Er^{3+} and Yb^{3+} ions belong to lanthanide series, and they have the similar ionic radius. Therefore, Er^{3+} and Yb^{3+} can be doped in KLW at a high concentration.

According to the literature data, some kinds of rare-earth double tungstates have been prepared in nanocrystalline state, such as $NaY(WO_4)_2$ [14] and $KEu(WO_4)_2$ [15]. In this paper, we focused attention on high Yb^{3+} and Er^{3+} concentration doped KLW nanoparticles prepared by Pechini method in order to study their crystal structure and investigate their luminescence properties. Unfortunately, the DC emissions of these samples were too weak to study. It could be attributed to the low phonon energy of the KLW crystal lattice.

2. Experimental procedure

The Yb^{3+} and Er^{3+} codoped KLW nanoparticles were prepared by the Pechini method. Lanthanum nitrate $La(NO_3)_3\cdot 6H_2O$ (99.99%), ytterbium nitrate $Yb(NO_3)_3\cdot 5H_2O$ (99.99%), erbium nitrate $Er(NO_3)_3\cdot 5H_2O$ (99.99%), ammonium paratungstate $(NH_4)_6W_7O_{24}\cdot 6H_2O$ (AR) and potassium carbonate K_2CO_3 (99.99%) were used as the source of metallic cations. Firstly, 1.5 mmol of the $Ln(NO_3)_3\cdot xH_2O$ (Ln=La, Er and Yb, and the molar ratio of La^{3+} ,Yb^{3+} and Er^{3+} depended on the doping concentration of Yb^{3+} and Er^{3+}) and separately, 0.4286 mmol of the ammonium paratungstate and 0.75 mmol of the potassium carbonate were dissolved in distilled water. Separately, 30 mmol of the citric acid (the molar ratio of the citric acid to K, W and Ln was 5:1) was dissolved in distilled water. After that, one-half of

* Corresponding author. Fax: +86 22 23501594.
E-mail address: suntq@nankai.edu.cn (T. Sun).

0022-4596/$ - see front matter © 2010 Elsevier Inc. All rights reserved.
doi:10.1016/j.jssc.2010.07.007

the citric acid solution was added to the rare-earth nitrate solution and another half was added to the potassium carbonate and ammonium paratungstate blended solution. Both of the solutions were stirred for 10 min, and then the two solutions were mixed together. To create rigid polyester net, 1.8 ml of the ethylene glycol was added (the molar ratio of the ethylene glycol to citric acid was 1:1). The mixture was dried at 80 °C for 1 h with constant stirring. Next, the mixture was transferred to the dryer and heated at 110 °C for 5 days. During this period, a brown resin was formed and the volume expanded several times. At last, the grinded resin was annealed at different temperatures ranging from 500 to 800 °C for 2 h to obtain the white nanoparticles of Yb^{3+} and Er^{3+} doped KLW.

The phase and crystallinity of the samples were analyzed by X-ray diffraction (NanoStar-C). Cu$K\alpha$ radiation was used in 2Θ ranges from 10° to 80° with a step of 0.02°.

The crystal structure analyses were made by the Rietveld method with the FullProf program using the profile function of pseudo-voigt with axial divergence asymmetry [16,17]. The effective 2Θ-range was limited to 10–120°.

Transmission electronic microscopy (TEM) images were taken on a 200 kV accelerating voltage by TeenaiG^{2}20s-TWIN.

The UC emission spectra were measured with an Edinburgh FSP920 fluorescence spectrophotometer with an external 980 nm LD as the excitation source.

3. Results and discussion

3.1. X-ray diffraction and TEM studies

Fig. 1 shows the X-ray diffraction patterns of the powders annealed at various temperatures and the standard XRD pattern of KLW (ICSD #95541). Single phase of KLW is formed in all the annealed samples according to the intense diffraction peaks. The average grain diameters can be estimated from the full width at half maximum (FWHM) of the diffraction peak ($2\Theta < 50°$) using the Scherrer equation which assumes the only cause of X-ray line broadening is the small crystallite size [18,19]:

$$D = K\lambda/(B\cos\Theta), \quad B^2 = a^2 - b^2$$

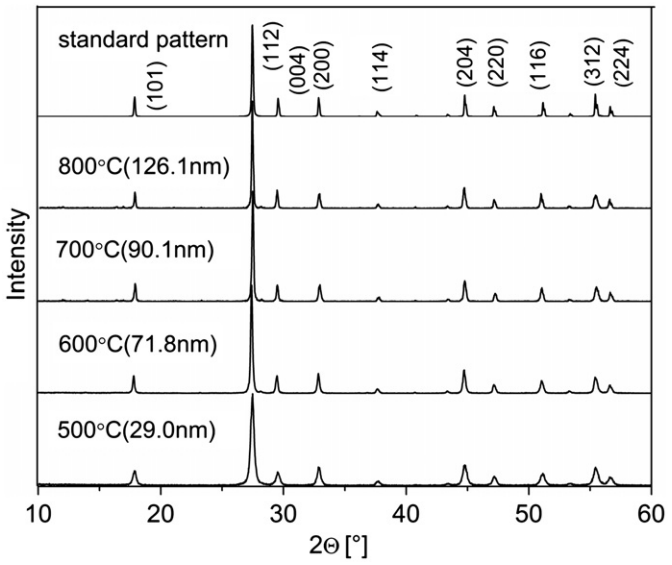

Fig. 1. X-ray powder diffraction patterns of samples annealed at different temperatures and X-ray diffraction pattern scheme for KLW (ICSD #95541). The average grain sizes of these samples are given in parentheses.

where D is the average grain size of the crystallite, λ is the X-ray wavelength (1.54056 Å), Θ is the Bragg angle of diffraction peak, K is the Scherrer constant and conventionally set to 1.0 [20–22], B is the FWHM of the true diffraction profile, a and b are the measured FWHM of the annealed powder and the standard sample (in our experiments, the standard sample is LaB_6), respectively. The results show that the average grain size of the samples annealed at 800 °C is bigger than 100 nm, and the samples annealed at 500 °C have much smaller grain size (about 29 nm) at the cost of poor crystallinity.

The TEM micrograph of the KLW samples annealed at 500 and 600 °C shows that the grain size of the synthesized powders is consistent with the calculation results, which increases with the increase of the annealing temperature (see Fig. 2). This figure also shows that the size distribution of the prepared samples is not homogeneous.

Fig. 3 shows the XRD patterns of the prepared samples codoped with constant 2 mol% Er^{3+} and different Yb^{3+} concentrations. The standard XRD pattern of $KYb(WO_4)_2$ (KYbW) which belongs to monoclinic system (ICSD #280877) [23] and the standard pattern of KLW (ICSD #95541) are also shown in Fig. 3 for comparing. When the Yb^{3+} doping concentration is higher than 10 mol%, more and more peaks which belong to monoclinic system appear with the increase of Yb^{3+} doping concentration. It is clear that the KYbW phase has formed when ytterbium is doped at a high concentration.

The structure of the samples was refined using the atomic parameters from KLW crystal as the starting data [24,25]. However, when the Yb^{3+} doping concentration was higher than 10 mol%, the structure could not be refined successfully. We have refined the 0, 5 and 10 mol% Yb^{3+} doped samples. The cell parameters and crystallite sizes are listed in Table 1. It is clear that both the cell parameters and crystallite size decrease with the increase of Yb^{3+} doping concentration. It can explain the phenomenon that the radius of Yb^{3+} ion is smaller than that of the La^{3+} ion. Fig. 4 shows the final Rietveld plot with a good agreement between the observed and calculated patterns. The atomic coordinates of 2 mol% Er^{3+} and 10 mol% Yb^{3+} codoped KLW nanoparticles are given in Table 2.

3.2. Luminescence studies

The UC emission spectra of the prepared samples are shown in Fig. 5. It is clear that the emission of the Yb^{3+} and Er^{3+} codoped sample is much stronger than that of the Er^{3+} single doped sample (both of the two samples were annealed at 700 °C for 2 h). The reason is that Yb^{3+} ions have a 10 times higher absorption cross section and a much broader peak than Er^{3+} ions at 980 nm. The green and the red fluorescent radiations correspond to the intra $4f$–$4f$ electronic transitions $^2H_{11/2}/^4S_{3/2} \rightarrow {}^4I_{15/2}$ and $^4F_{9/2} \rightarrow {}^4I_{15/2}$ of Er^{3+}, respectively.

The emission spectra of KLW (10 mol%-Yb and 2 mol%-Er codoped) annealed at 600, 700 and 800 °C are shown in Fig. 6. It shows that the intensity of the UC emission increases with the increase of the annealing temperature. Different grain size is the only difference among these samples (in Fig. 1). It is obvious that the increase of the particle size is helpful to the UC emission.

Fig. 7 shows the energy level diagrams of Yb^{3+} and Er^{3+} ions [8]. The Yb^{3+} ions can be excited to $^2F_{5/2}$ state by absorbing one 980 nm laser photon. For the green emission, the Er^{3+} ions jump from the ground state to the long-lived $^4I_{11/2}$ state (ET1), and then jump from $^4I_{11/2}$ state to $^4F_{7/2}$ state (ET2). Subsequently, the Er^{3+} ions at $^4F_{7/2}$ state relax rapidly to $^4H_{11/2}$ or $^4S_{3/2}$ state by releasing several phonons, from which the green emissions arise. There are two channels for red emission: (a) the Er^{3+} ions at $^4I_{11/2}$ state

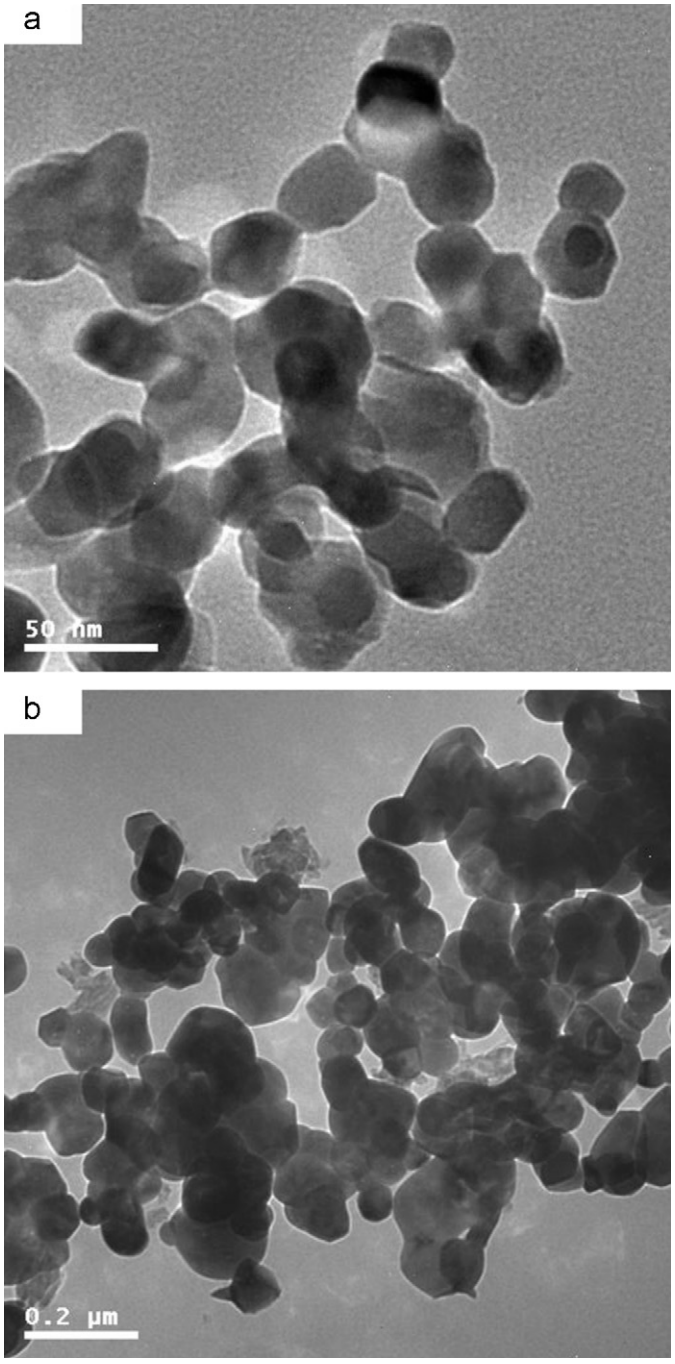

Fig. 2. TEM photographs of KLW nanocrystalline powders annealed at 500 °C (a) and 600 °C (b) for 2 h.

relax to $^4I_{13/2}$ state and then jump to $^4F_{9/2}$ state (ET3); (b) the $^4F_{9/2}$ state is populated by the non-radiative contribution from the above excited state $^4S_{3/2}$. All the transitions can finish by absorbing one 980 nm laser photon or absorbing the energy transmitted from Yb^{3+} ions in the codoped samples, and the latter is the dominant process. So the UC emissions of the codoped samples should be much stronger. The Er^{3+} energy level diagram shows that both the energy gap between $^4I_{11/2}$ and $^4I_{13/2}$ state (about 3500 cm^{-1}) and the gap between $^4S_{3/2}$ and $^4F_{9/2}$ state (about 3200 cm^{-1}) [8] are about four times of the phonon energy of KLW lattices (about 900 cm^{-1}) [26], so only a small proportion of Er^{3+} ions can populate at $^4F_{9/2}$ state and the red emission

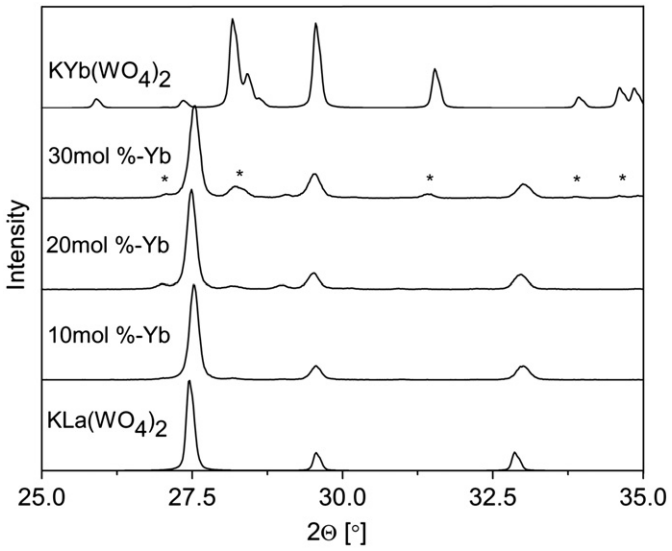

Fig. 3. XRD patterns of KLW samples doped with constant 2 mol% Er^{3+} and different Yb^{3+} concentrations (annealed at 700 °C for 2 h). The X-ray diffraction pattern schemes for KLW (ICSD #95541) and KYbW (ICSD #280877) are showed for comparing.

Table 1
Cell parameters and crystallite size of KLW nanoparticles doped with constant 2 mol% Er^{3+} and different Yb^{3+} concentrations (annealed at 700 °C for 2 h).

Yb^{3+} concentration (mol%)	Cell parameters		Crystallite size (nm)
	$a=b$ (Å)	c (Å)	
0	5.440087(10)	12.12601(2)	81.5(7)
5	5.432759(10)	12.10329(3)	75.4(6)
10	5.430908(10)	12.09500(3)	71.8(5)

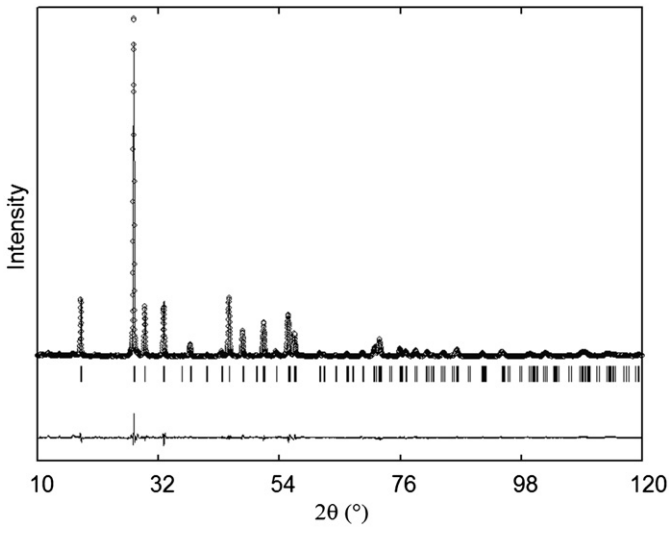

Fig. 4. Final Rietveld plot for KLW (codoped with 2 mol% Er^{3+} and 10 mol% Yb^{3+}). Small circles (○) are the experimental values, and the continuous lines stand for the calculated pattern; vertical bars (|) correspond to the position of Bragg peaks. The bottom trace is the difference between the experimental and calculated intensity values.

should be much weaker than the green emission, which agrees with the phenomenon showed in Fig. 5.

The mechanisms of the UC emission suggest that all the three bands of UC emissions are two-photon process. The pump power

Table 2
Refined structural parameters for KLW (codoped with 2 mol% Er^{3+} and 10 mol%Yb^{3+}) at room temperature, space group $I4_1/a$, R_p=8.58, R_{wp}=11.6, R_{Bragg}=6.83.

Atom	Site	*x*	*y*	*z*	*Biso*	*Occ*
W	4*a*	0.00000	0.25000	0.12500	2.19(2)	1.00
La	4*b*	0.50000	0.75000	0.12500	2.26(4)	0.44
Yb	4*b*	0.50000	0.75000	0.12500	2.26(4)	0.05
Er	4*b*	0.50000	0.75000	0.12500	2.26(4)	0.01
K	4*b*	0.50000	0.75000	0.12500	2.26(4)	0.50
O	16*f*	0.2685(3)	0.3930(4)	0.4506(2)	5.5(2)	1.00

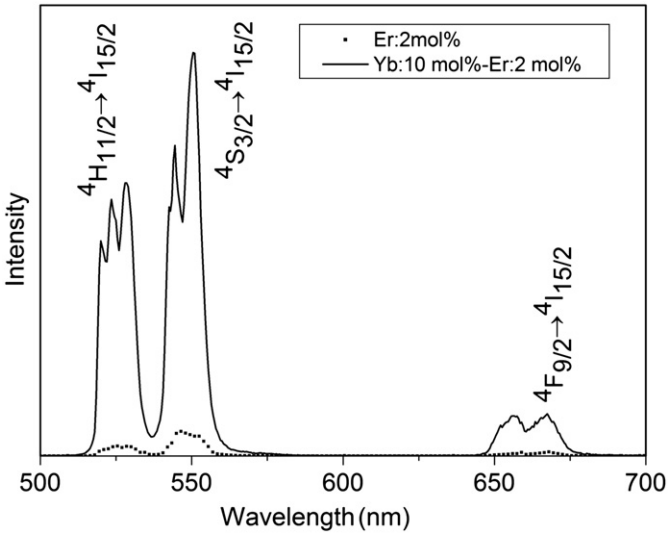

Fig. 5. UC emission spectra of 10 mol% Yb^{3+}–2 mol% Er^{3+} codoped KLW nanoparticles (solid line) and the 2 mol% Er^{3+} single doped KLW nanoparticles (dotted line).

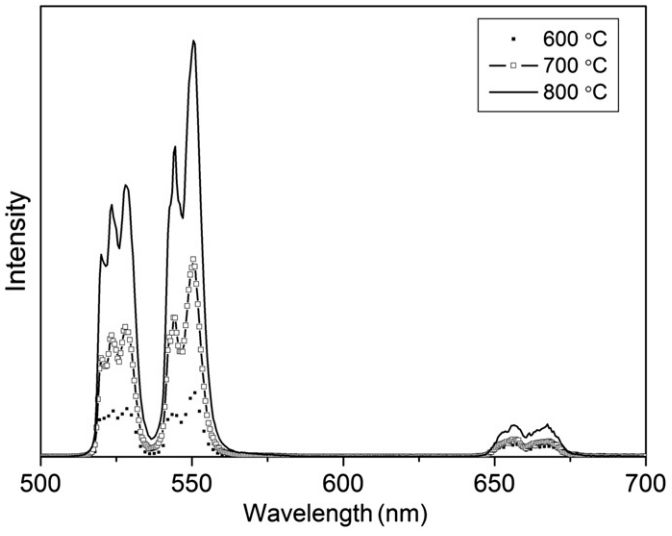

Fig. 6. UC emission spectra of KLW (10 mol%-Yb and 2 mol%-Er codoped) annealed at 600 °C (dotted line), 700 °C (line+symbol) and 800 °C (solid line).

dependence of the UC emissions has been measured to prove the above deduction. The power dependence of 10 mol% Yb^{3+} and 2 mol% Er^{3+} codoped KLW nanoparticles are shown in Fig. 8, in which all the three slopes are about 2 (slope=1.914, 1.860, 1.794 for 528, 550 and 656 nm wavelength emissions, respectively). The results are consistent with the UC emission mechanisms.

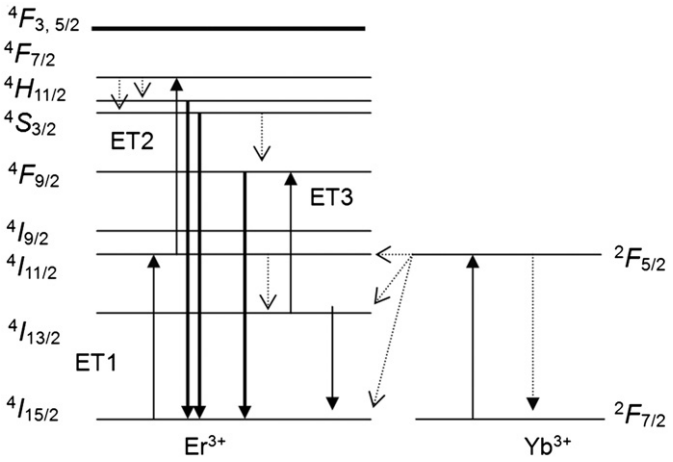

Fig. 7. Energy level diagram of Er^{3+} and Yb^{3+} in KLW nanocrystals doped with Er^{3+} and Yb^{3+} under excitation of 980 nm LD.

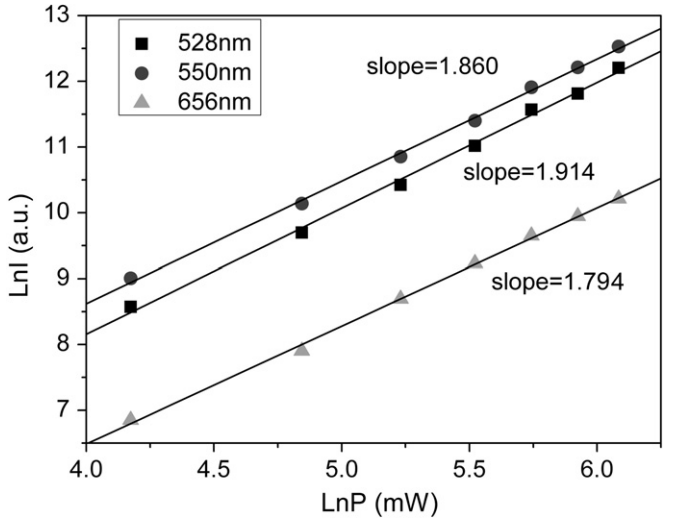

Fig. 8. Pump power dependence of all the three bands of UC emission spectra of KLW codoped with 10 mol% Yb^{3+} and 2 mol% Er^{3+}.

Fig. 9 shows the dependence of the luminescence intensity of the codoped KLW nanoparticles on doping concentration of Yb^{3+} ions by monitoring the emission of $^4S_{3/2}\rightarrow{}^4I_{15/2}$ transition at 550 nm (the doping concentration of Er^{3+} is 1, 1.5 and 2 mol% separately). The luminescence intensity increased with the increase of Yb^{3+} doping concentration and reached the maximum at 10 mol%, and then decreased with the increase of Yb^{3+} doping concentration. It may be induced by the combined action of the saturation of $^4I_{11/2}$ (Er^{3+}) state and formation of KYW phase when Yb^{3+} doped at a high concentration. Fig. 9 also shows that the luminescence intensity of the 1.5 mol% Er^{3+} doped sample is slightly stronger than others when Yb^{3+} doped at the same concentration.

4. Conclusion

Yb^{3+} and Er^{3+} doped KLW nanoparticles have been prepared by Pechini method. The average grain size of the nanocrystalline increases rapidly with the increase of the annealing temperature and exceeds 100 nm just above 800 °C. The monoclinic phase has been observed when the Yb^{3+} ions doped at a high concentration. A highly green UC emission of Yb^{3+}–Er^{3+} codoped KLW

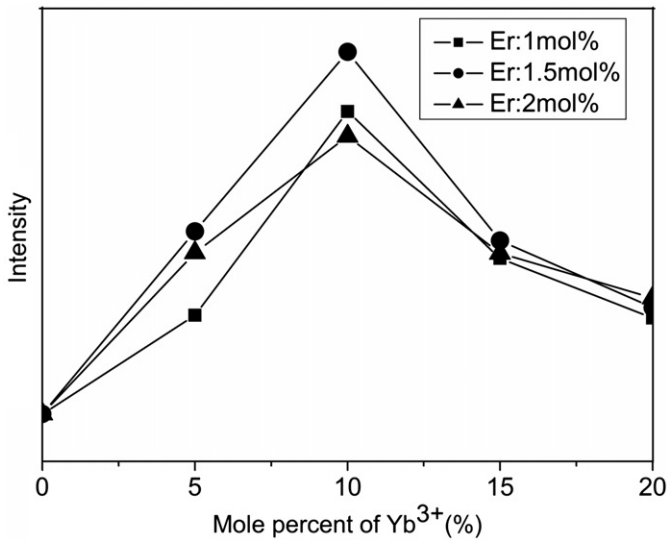

Fig. 9. Relationship between the luminescence intensity of the Er–Yb codoped KLW powders and mole percent of Yb^{3+} ions (doping concentration of Er^{3+} is 1, 1.5 and 2 mol%, separately).

nanoparticles has been observed, and the UC luminescence mechanisms suggest that all the three bands of UC emissions are two-photon process. The best doping concentration of KLW for UC emission is about 10 mol% Yb–1.5 mol% Er.

Acknowledgments

This work is supported by the National Natural Science Foundation of China (Grant nos. 50702026 and 60778038) and Specialized Research Fund for the Doctoral Program of Higher Education (SRFDP) (Grant no. 20070055063).

References

[1] C. Cascales, A.M. Blas, M. Rico, V. Volkov, C. Zaaldo, Opt. Mater. 27 (2005) 1672–1680.
[2] I. Nikolov, X. Mateos, F. Guell, J. Massons, V. Nikolov, P. Peshev, E. Diaz, Opt. Mater. 25 (2005) 53–58.
[3] K. Hermanowicz, J. Phys.: Condens. Matter 18 (2006) 10601–10616.
[4] K. Takaichi, H Yagi, A. Shirakawa, K. Ueda, S. Hosokawa, T. Yanagitani, A.A Kaminskii, Phys. Status Solidi A 202 (2005) R1.
[5] A.A. Kaminskii, Phys. Status Solidi A 200 (2003) 215–296.
[6] I. Kasacki, T. Suzuki, H.U. Anderson, P. Colomban, Solid State Ionics 149 (2002) 99–105.
[7] I. Kosacki, H.U. Anderson, Encyclopedia of Materials: Science and Technology, vol. 4, Elsevier, New York, 2001, pp. 3609–3617.
[8] G.Y. Chen, G. Somesfalean, Y. Liu, Z.G. Zhang, Q. Sun, F.P. Wang, Phys. Rev. B 75 (2007) 195–204.
[9] M. Maczka, K. Hermanowicz, P.E. Tomaszewski, M. Zawadzki, J. Hanuza, Solid State Sci. 10 (2008) 61–68.
[10] R. Kasuya, T. Isobe, S. Yamao, Jpn. J. Appl. Phys. 9 (2007) 5879–5884.
[11] X.M. Han, Z.B. Lin, Z.S. Hu, G.F. Wang, Mater. Res. Innovations 6 (2002) 118–121.
[12] G. Wang, M. He, Z. Luo, Mater. Res. Bull. 26 (1991) 1086–1093.
[13] M. He, G. Wang, Z. Luo, W. Chen, S. Lu, Q. Wu, Mater. Res. Innovations 2 (1999) 345–349.
[14] N. Xue, X.P. Fan, Z. Wang, M.Q. Wang, Mater. Lett. 61 (2007) 1576–1579.
[15] L. Macalik, P.E. Tomaszewski, R. Lisiecki, J. Hanuza, J. Solid State Chem. 181 (2008) 2591–2600.
[16] T. Roisnel, J. Rodriguez-Carvajal, WinPLOTR, a graphic tool for powder diffraction, version January 2006.
[17] J. Rodriguez-Carvajal, FULLPROF: a program for Rietveld refinement and pattern matching analysis, in: Abstracts of the Statellite Meeting on Powder Diffraction of the XVth Congress of IUCr, Toulouse, France, 1990, p. 127.
[18] A.L. Patterson, Phys. Rev. 56 (1939) 978–982.
[19] S.B. Qadri, E.F. Skelton, D. Hsu, A.D. Dinsmore, J. Yang, H.F Gray, B.R. Ratna, Phys. Rev. B 60 (1999) 9191–9193.
[20] S. Chattopadhyay, P. Ayyub, V.R. Palkar, M. Multani, Phys. Rev. B 52 (1995) 13177–13183.
[21] J.I. Langford, A.J.C. Wilson, J. Appl. Crystallogr. 11 (1978) 102–113.
[22] F. Toney, J. Giijo, M. Siby, P.R. Rejikumar, N.V. Unnikrishnan, J. Sol–Gel Sci. Technol. 41 (2007) 163–168.
[23] W. Strek, A. Bednarkiewicz, P.J. Deren, J. Lumin. 92 (2001) 229–235.
[24] X. Han, G.F. Wang, J. Cryst. Growth 249 (2003) 167–171.
[25] X. Han, G.F. Wang, Mater. Res. Innovations 6 (2002) 235–237.
[26] J. Hanuza, L. Macalik, M. Maczka, E.T.G. Lutz, J.H. van der Maas, J. Mol. Struct. 511–512 (1999) 85–106.